Triple-α continuum structure and Hoyle resonance of ^{12}C using the hyperspherical slow variable discretization

Hiroya Suno*
RIKEN Advanced Institute for Computational Science, Kobe 650-0047, Japan, and RIKEN Nishina Center, Wako 351-0198, Japan

Yasuyuki Suzuki
Department of Physics, Niigata University, Niigata 950-2181, Japan, and RIKEN Nishina Center, Wako 351-0198, Japan

Pierre Descouvemont
Physique Nucléaire Théorique et Physique Mathématique, Code Postal 229, Université Libre de Bruxelles (ULB), B-1050, Brussels, Belgium
(Received 10 October 2014; published 13 January 2015)

We develop a method for calculating the bound and continuum energy spectrum of three particles interacting through both short-range and Coulomb potentials. Our method combines hyperspherical coordinates with the slow variable discretization approach. A complex absorbing potential is employed to describe accurately the continuum wave functions. The method is well known in atomic and molecular physics. It is extended here to nuclear physics, with a special emphasis on the long-range Coulomb interaction. The method is applied to compute the energy spectrum of ^{12}C in a 3α-particle model, focusing on an accurate calculation of the Hoyle resonance width of the narrow near-threshold $J^\pi_n = 0^+_2$ state, which plays an important role in stellar nucleosynthesis. We employ an effective α-α interaction potential which reproduces both the energy and width of ^{8}Be, while a three-body force is added in order to fix the ^{12}C energy levels at the experimental values. We also analyze the structure of the bound and resonance states by calculating the wave functions and one-dimensional distribution functions.

DOI: 10.1103/PhysRevC.91.014004 PACS number(s): 21.45.−v, 21.60.−n, 27.20.+n, 21.10.Tg

I. INTRODUCTION

Systems involving three particles interacting through the Coulomb potential are complicated problems that have not yet been completely solved or understood. The main difficulty when solving the Schrödinger equation for three charged particles resides in describing reliably the three-body continuum wave function. The treatment of the three-body continuum wave function for such systems is of great importance in nuclear, atomic, and molecular physics. One such problem is the description of the astrophysically important continuum states in ^{12}C as a system of three α particles [1,2]. The 0^+_2 state (Hoyle state) lies above the three-body dissociation threshold and therefore requires correct continuum conditions of the three-body Coulomb problem. It has been intensively studied in the past [3–9]. This near-threshold three-body resonance, together with the low-energy α-α resonance of ^{8}Be, is thought to be of key importance for the description of the famous triple-α reaction as the only explanation for the observed abundance of ^{12}C in the universe [10].

In the present work, we develop a method for calculating the bound and continuum energy spectrum of three α particles interacting through the Coulomb potential. Our method has been extensively used in atomic and molecular three-body problems [11,12]; it combines the hyperspherical coordinates [13] with the slow variable discretization (SVD) approach. The boson permutation symmetry is enforced using a modified version of the Smith-Whitten coordinate system [14,15]. The SVD approach was introduced by Tolstikhin *et al.* [11] to overcome the difficulties arising from the adiabatic expansion scheme—the hyper-radial coupled-channel equations become stiff to integrate when very sharp avoided crossings take place between potential curves, as will be seen between the $\alpha + {}^8$Be channel and the $\alpha + \alpha + \alpha$ three-body continuum channels in the three-α system. A complex absorbing potential (CAP) is introduced in the asymptotic region in order to absorb the dissociating flux [16,17], allowing us to obtain resonance positions and widths as real and imaginary parts of complex eigenenergies from the resulting system's Hamiltonian without knowledge about the asymptotic form of the adiabatic potential curves. For low-energy resonances, the approach is more efficient than the complex scaling method [18], where physical resonances cannot be clearly separated from the continuum, especially when they have very narrow widths.

Our method will be applied to calculate the continuum (and bound) spectra for three α particles in ^{12}C. The main attention is focused on an accurate calculation of the resonance width of the narrow $J^\pi_n = 0^+_2$ state. Convergence of the resonance properties with respect to the basis size and the CAP parameter will be carefully checked. A modified version of the Ali-Bodmer potential [19] is adopted to describe the α-α interaction while the three-body potential is employed to adjust the bound and resonance energy levels at the experimental values.

The organization of this paper is as follows: Section II presents the theoretical approach. In Sec. III, we discuss the results and analyses of the system under study. We finally conclude and summarize in Sec. IV.

*suno@riken.jp

II. METHOD

A. Slow variable discretization (SVD) approach

We solve the Schrödinger equation for three interacting particles combining the hyperspherical coordinates [13] with the SVD approach [11]. The method employed here was applied to atomic three-body systems like Ne_3 and HeNeH in Refs. [20,21]. Since the method is described in details in those references, we give mainly an outline here. After the usual separation of the center-of-mass motion, we describe the three-body problem using a modified version of the Smith-Whitten democratic hyperspherical coordinates $(R,\Omega) \equiv (R,\theta,\varphi,\alpha,\beta,\gamma)$ [14,15,22–25]. We first introduce the mass-scaled Jacobi coordinates [26,27] for three identical particles:

$$\vec{\rho}_1 = \frac{3^{1/4}}{2^{1/2}}(\vec{r}_2 - \vec{r}_1), \quad \vec{\rho}_2 = \frac{2^{1/2}}{3^{1/4}}\left(\vec{r}_3 - \frac{\vec{r}_1 + \vec{r}_2}{2}\right), \tag{1}$$

with $\vec{r}_i$ being the position coordinate of particle i. The hyperradius $R = (\rho_1^2 + \rho_2^2)^{1/2}$, $R \in [0,\infty)$, describes the global size of the three-particle system (we can also write $R^2 = \sqrt{3}\sum_{i=1}^{3}(\vec{r}_i - \vec{R}_{\rm cm})^2$ with $\vec{R}_{\rm cm}$ being the center-of-mass coordinate), while the Euler angles (α,β,γ) specify the orientation of the body-fixed frame in space. The axes of this frame lie along the principal axes of inertia: The z axis is parallel to $\vec{\rho}_1 \times \vec{\rho}_2$ and the x axis is associated with the smallest moment of inertia. The two hyperangles (θ,φ) describe the shape of the triangle formed by the three particles and are defined by

$$\begin{aligned}
(\vec{\rho}_1)_x &= R\cos(\pi/4 - \theta/2)\cos(\varphi/2 + \pi/3),\\
(\vec{\rho}_1)_y &= R\sin(\pi/4 - \theta/2)\sin(\varphi/2 + \pi/3),\\
(\vec{\rho}_2)_x &= -R\cos(\pi/4 - \theta/2)\sin(\varphi/2 + \pi/3),\\
(\vec{\rho}_2)_y &= R\sin(\pi/4 - \theta/2)\cos(\varphi/2 + \pi/3).
\end{aligned} \tag{2}$$

The hyperangles θ and φ span the ranges $[0,\pi/2]$ and $[0,2\pi]$, respectively, after requiring the wave function to be single valued [15]. As we will see below, the hyperangle φ can be further restricted to the range $[0,\pi/3]$ when the three particles are indistinguishable.

In terms of a rescaled wave function $\psi = R^{5/2}\Psi$, with Ψ being the usual wave function, the Schrödinger equation for three particles interacting through the potential $V(R,\theta,\varphi)$ reads

$$\left[-\frac{\hbar^2}{2\mu}\frac{\partial^2}{\partial R^2} + \frac{\Lambda^2 + \frac{15}{4}\hbar^2}{2\mu R^2} + V(R,\theta,\varphi)\right]\psi(R,\Omega) = E\psi(R,\Omega), \tag{3}$$

where μ is the three-body reduced mass ($\mu = m/\sqrt{3}$ for three identical particles of mass m). Λ^2 is the squared "grand angular momentum operator" [15,23] and is given by

$$\begin{aligned}
\Lambda^2 = &-\frac{4\hbar^2}{\sin 2\theta}\frac{\partial}{\partial\theta}\sin 2\theta\frac{\partial}{\partial\theta} + \frac{4}{\sin^2\theta}\left(i\hbar\frac{\partial}{\partial\varphi} - \cos\theta\frac{J_z}{2}\right)^2\\
&+ \frac{2J_x^2}{1-\sin\theta} + \frac{2J_y^2}{1+\sin\theta} + J_z^2.
\end{aligned} \tag{4}$$

The operators (J_x, J_y, J_z) are the body-fixed frame components of the total angular momentum $\vec{J}$. The Schrödinger equation (3) must be solved for a given set of quantum numbers (J,M,π): J is the total angular momentum, M its projection on a space-fixed axis, and π the parity with respect to the inversion of nuclear coordinates. The interaction potential $V(R,\theta,\varphi)$ in Eq. (3) is taken to be a sum of two-body potentials and a three-body interaction, i.e.,

$$V(R,\theta,\varphi) = v(r_{12}) + v(r_{23}) + v(r_{31}) + w(r_{12},r_{23},r_{31}), \tag{5}$$

where r_{ij} are the interparticle distances. In terms of the hyperspherical coordinates, they are

$$\begin{aligned}
r_{12} &= 3^{-1/4}R[1 + \sin\theta\cos(\varphi + 2\pi/3)]^{1/2},\\
r_{23} &= 3^{-1/4}R[1 + \sin\theta\cos\varphi]^{1/2},\\
r_{31} &= 3^{-1/4}R[1 + \sin\theta\cos(\varphi - 2\pi/3)]^{1/2}.
\end{aligned} \tag{6}$$

The motion in R is first treated by introducing a set of finite-element methods–discrete variable representation (FEM-DVR) points and weights (r_l,ω_l) $(l = 1,2,\ldots,L)$. These are generated by dividing the hyper-radial range with a set of N grid points and by further subdividing each of the intervals with $\mathcal{M}$th-order shifted and scaled Gauss-Lobatto quadrature points [28]. The total number of grid points then equals $L = (\mathcal{M} - 1)(N - 1) + 1$ with any two repeated points being merged into a single point. The FEM-DVR basis functions $\chi_l(R)$ $(l = 1,2,\ldots,L)$ are constructed from the FEM-DVR points and weights using the Lobatto shape functions [29] and satisfy $\chi_l(r_{l'}) = \omega_l^{-1/2}\delta_{ll'}$. For details, see Ref. [20].

Combined with the FEM-DVR basis, the SVD approach consists of seeking for solutions of the Schrödinger equation in the form

$$\psi(R,\Omega) = \sum_{\nu=1}^{\infty}\sum_{l=1}^{L} c_{l\nu}\chi_l(R)\Phi_\nu(r_l;\Omega), \tag{7}$$

where $\Phi_\nu(r_l;\Omega)$ are the channel functions, which are solutions of the adiabatic equation at a fixed hyper-radius $R = r_l$:

$$\left[\frac{\Lambda^2 + \frac{15}{4}\hbar^2}{2\mu R^2} + V(R,\theta,\varphi)\right]\Phi_\nu(R;\Omega) = U_\nu(R)\Phi_\nu(R;\Omega), \tag{8}$$

with $U_\nu(R)$ being the adiabatic eigenenergies, or adiabatic hyperspherical potential curves. The SVD approach in Eq. (7) is adopted instead of the adiabatic expansion approach since the latter approach cannot describe accurately the nonadiabatic couplings when very sharp avoided crossings take place between the potential curves. In standard hyperspherical calculation, the wave function (7) is expanded over hyperspherical harmonics (K harmonics) [13,30]. The expansion, however, is known to converge slowly, in particular for three-body continuum states [31]. We will show later that the convergence over ν [see Eq. (7)] is much faster. For solution of the adiabatic equation, see Appendix A.

Insertion of ψ from Eq. (7) into the Schrödinger equation from Eq. (3) results in a set of hyper-radial coupled-channel equations:

$$\sum_{\nu'=1}^{\infty}\sum_{l'=1}^{L}\mathcal{T}_{ll'}\mathcal{O}_{\nu l,\nu' l'}c_{l'\nu'} + U_\nu(r_l)c_{l\nu} = Ec_{l\nu}, \tag{9}$$

where $\mathcal{O}_{\nu l,\nu' l'} = \langle\langle \Phi_\nu(r_l;\Omega)|\Phi_{\nu'}(r_{l'};\Omega)\rangle\rangle$ are the overlap matrix elements between adiabatic channels defined at different quadrature points $R = r_l$ and $r_{l'}$, and the double bracket denotes integration over the five angular coordinates Ω. $\mathcal{T}_{ll'}$ are the hyper-radial kinetic energy matrix elements and are given in Ref. [20].

B. Complex absorbing potential (CAP)

A CAP is used to simulate an infinite hyper-radial grid. CAPs are defined to be nonzero only in the asymptotic region, converting the outgoing waves into exponentially decreasing functions, thus allowing for the use of L^2 (basis expansion) methods. The functional form and parameters of CAPs need to be optimized in order to minimize transmission and reflection properties of these potentials. A CAP is purely imaginary and must be added to the adiabatic potentials $U_\nu(R)$, so that

$$U_\nu(R) \to U_\nu(R) - iW_\nu(R). \tag{10}$$

This transforms the coupled-channel equations (9) into a complex symmetric generalized eigenvalue problem. The eigenenergies corresponding to the bound states do not change under this transformation, but those corresponding to the resonances are obtained in the form

$$E = E^r - i\Gamma/2, \tag{11}$$

where E^r is the resonance position and Γ is the width (inverse of lifetime). The eigenenergies corresponding to the continuum states may depend on the form of a CAP and its parameters, but the resonance positions and widths should not. Various CAPs were proposed and tested in the past (see Refs. [32–34] and references therein), while Blandon *et al.* [12] combined CAPs with the hyperspherical SVD approach.

In the present work, we adopt the transmission-free (TF) CAP proposed by Manolopoulos [16] and Gonzalez-Lezana *et al.* [17] and tested by Grozdanov *et al.* [35]. The main advantage of this potential is its ability to be used for a wide range of kinetic energies of interest without the necessity of optimizing any of its parameters. The TF-CAP is given by

$$W(R) = \begin{cases} 0, & R < R_a, \\ \frac{4E_{\min}}{C^2}\left[\frac{1}{(1-x)^2} + \frac{1}{(1+x)^2} - 2\right], & R_a \leqslant R < R_{\max}, \end{cases} \tag{12}$$

where $C = 2.62206$. $E_{\min}$ is the lowest scattering energy of interest, R_a defines the border between the interaction and asymptotic regions, and $x = (R - R_a)/D$. The absorption length $D = R_{\max} - R_a$ is taken to be equal to the de Broglie wavelength corresponding to $E_{\min}$. We mention here that it would be possible to introduce channel-dependent CAPs $W_\nu(R)$ instead of a channel-independent CAP $W(R)$, but the latter one is adequate in our case, since, as will be seen, all the adiabatic potential curves approach one single threshold, i.e., the three-body dissociation threshold. In Appendix B, we illustrate the method with the simple α-α system.

III. RESULTS AND DISCUSSION

A. Conditions of the calculations

For the two-body potential $v(r)$, we use the sum of an $\alpha + \alpha$ potential and the Coulomb potential,

$$v(r) = v_{\alpha\alpha}(r) + v_C(r), \tag{13}$$

with

$$v_{\alpha\alpha}(r) = 125e^{-r^2/1.53^2} - 30.18e^{-r^2/2.85^2} \tag{14}$$

and

$$v_C(r) = \frac{4e^2}{r}\mathrm{erf}(0.60141r). \tag{15}$$

Here, the potential parameters are given in units of MeV for energy and femtometers for length. The mass m of α particle is set to $\hbar^2/m = 10.5254408$ MeV fm^2 and the charge constant e^2 to 1.4399644 MeV fm. $v_{\alpha\alpha}$ is the S-wave potential used in Ref. [3] that is obtained by slightly modifying the Ali-Bodmer potential [19]. Note that the above two-body potential ($v_{\alpha\alpha} + v_C$) gives one S-wave ^{8}Be resonance state, of which the position and width are given respectively by $\epsilon_0^r = 88.83966$ keV and $\gamma_0 = 5.66$ eV. These values are determined by solving the two-body Schrödinger equation using fifth-order basis splines and a TF-CAP. These resonance position and width are in good agreement with experimental data [36]: 91.8 keV and 5.57 ± 0.25 eV. In what follows we assume that the $\alpha + \alpha$ potential of Eq. (13) acts on all partial waves of the α-α relative motion. This indicates that our potential is slightly too repulsive for D and G waves, but it is readjusted by the three-body potential w. The three-body potential w can be taken to be a simple Gaussian

$$w(R) = w_3^{(J\pi)} \exp\left(-R^2/b_3^2\right), \tag{16}$$

which depends only on the hyper-radius R. The range parameter is taken to be $b_3 = 2.58$ fm, while the strength parameter $w_3^{(J\pi)}$ will be adjusted to reproduce the desired energy level for a given J^π. Since the three-body potential depends only on the hyper-radius R, we can omit it when solving the adiabatic equation (8) and incorporate it instead into the hyper-radial coupled-channel equations (9). Figure 1 displays two-dimensional contour plot of the potential energy surface without three-body term, $\sum_{i<j}^3 v(r_{ij})$, at a fixed hyper-radius $R = 10$ fm as a function of the hyperangles θ and φ. Due to the presence of three identical particles, the potential energy surface is invariant under translation by $2\pi/3$ in the φ direction. In addition, it is invariant under reflection about $\pi/3$. The two-body coalescent points with $r_{12} = 0$, $r_{23} = 0$, and $r_{31} = 0$ correspond respectively to $(\theta,\varphi) = (\pi/2,\pi/3)$, $(\pi/2,\pi)$, and $(\pi/2,5\pi/3)$, as has been explained above. The contour lines surround these coalescent points in the form of ellipses. As R increases, the contour lines shrink and approach the coalescent points.

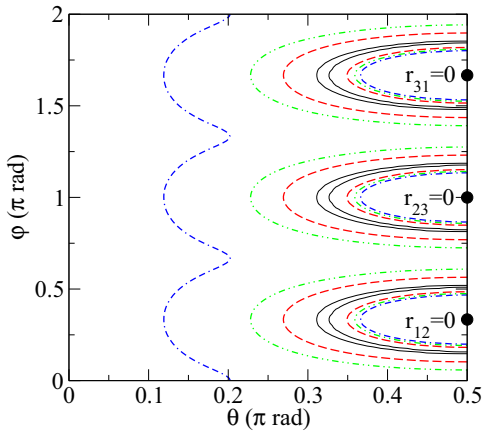

FIG. 1. (Color online) Two-dimensional contour plot of the potential energy surface without three-body term, $\sum_{i<j}^{3} v(r_{ij})$, at a fixed hyper-radius $R = 10$ fm as a function of the hyperangles θ and φ for the three-α system. The solid lines show the lowest contour line shown here (-4 MeV); the dashed lines show the second lowest contour line (-2 MeV). The other lines correspond to 0 MeV and 2 MeV. The closed circles indicate the two-body coalescent points.

B. Adiabatic potential curves

In the present work, we restrict ourselves to the $J^\pi = 0^+$ and 2^+ symmetries, although the other symmetries can be treated easily. Figures 2(a) and 2(b) show the lowest adiabatic hyperspherical potential curves for the three-α system in those symmetries. These potential curves are calculated with the three-body potential (16) with $w_3^{(0+)} = -152.2$ MeV for $J^\pi = 0^+$ and $w_3^{(2+)} = -179.5$ MeV for 2^+. They are chosen to reproduce the energies of the 0_2^+ and 2_1^+ states. All these potential curves correspond asymptoticaly to the three-body continuum states and approach the three-body dissociation threshold $U_\nu(R) \to 0$ in the limit of large hyper-radii $R \to \infty$.

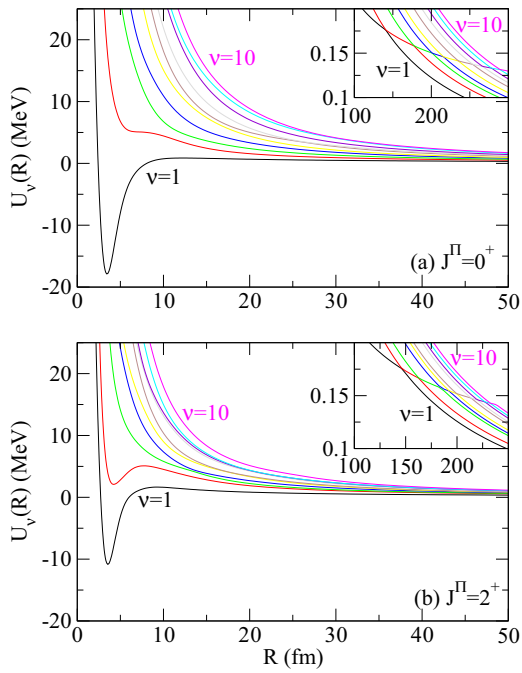

FIG. 2. (Color online) The 10 lowest adiabatic hyperspherical potential curves $U_\nu(R)$ of the three-α system for (a) $J^\pi = 0^+$ and (b) $J^\pi = 2^+$. In both panels (a) and (b), the inset shows the crossings between the potential curves corresponding to the ^{8}Be resonance.

Convergence of the potential curves with respect to the basis splines in θ and φ can be determined by computing them for different numbers of grid points N_θ and N_φ from which they are generated. To do so, we choose the $J^\pi = 0^+$ symmetry and calculate the several lowest eigenenergies at a fixed hyper-radius $R = 20$ fm. If we compare the 25 lowest adiabatic eigenenergies for $(N_\theta, N_\varphi) = (40,60)$ and $(60,90)$, the maximum of the fractional differences $|(U_\nu^{(40,60)} - U_\nu^{(60,90)})/U_\nu^{(40,60)}|$ ($\nu = 1 - 25$) between the adiabatic eigenenergies from the (40,60) and (60,90) is found to be 5×10^{-11}. This implies that these eigenenergies are converged to more than ten significant digits with respect to the basis splines in θ and φ, and we use therefore $(N_\theta, N_\varphi) = (40,60)$ for all the calculations throughout this work.

In Fig. 2, we can observe a series of sharp avoided crossings for both the $J^\pi = 0^+$ and 2^+ states; see the insets. These avoided crossings are due to the slowly decreasing two-cluster $\alpha + {}^8$Be channel (the lowest potential curve at small R) that comes across the rapidly decreasing three-body $\alpha + \alpha + \alpha$ channels. The two-cluster potential curve approaches asymptotically the ^{8}Be ground-state energy level and is expressed as $U_{\alpha+{}^8\mathrm{Be}}(R) = \epsilon_0^r + \tilde{q}R^{-1} + O(R^{-2})$, with ϵ_0^r being the ^{8}Be energy level and $\tilde{q}$ the Coulomb parameter $\tilde{q} = 8 \times 2^{1/2} e^2 / 3^{1/4}$. Such avoided crossings therefore take place whenever the two-body subsystem supports a resonance energy level above the three-body dissociation threshold. The adiabatic channel functions certainly exchange their characteristics through these avoided crossings. This can be seen by computing the contributions of the different terms in the adiabatic Hamiltonian to the potential curves as functions of the hyper-radius R. Figures 3(a) and 3(b) show the contributions of the centrifugal potential $\langle\langle \Phi_\nu | \Lambda^2/(2\mu R^2) | \Phi_\nu \rangle\rangle$, the nuclear potentials $\langle\langle \Phi_\nu | \sum_{ij} v_{\alpha\alpha}(r_{ij}) | \Phi_\nu \rangle\rangle$, and the Coulomb potentials $\langle\langle \Phi_\nu | \sum_{ij} v_C(r_{ij}) | \Phi_\nu \rangle\rangle$ to the two lowest potential curves $U_1(R)$ and $U_2(R)$ for 0^+, from which we see an avoided crossing occurring at $R \approx 140$ fm. The three-body term is found to be negligibly small compared with the other contributions. At hyper-radii smaller than this value, the lowest curve $U_1(R)$ exhibits the nature of the two-cluster $\alpha + {}^8$Be channel (the centrifugal potential, the nuclear potentials, and the Coulomb potentials comparable in magnitude with each other), whereas the second curve $U_2(R)$ shows the characteristics of a three-body $\alpha + \alpha + \alpha$ continuum channel (the Coulomb potentials are by far dominant over the centrifugal potential and the nuclear potentials). At hyper-radii larger than $R \approx 140$ fm, these two different characteristics are found to be exchanged, and the lowest curve behaves as a three-body channel and the second lowest one as the two-cluster channel. We can also see that a similar exchange takes place between $U_2(R)$ and $U_3(R)$ at $R \approx 180$ fm, beyond which $U_2(R)$ shows again the nature of a three-body channel.

The asymptotic behavior of the three-body curves with the Coulomb interaction is not well known in contrast to three-body systems only with short-range potentials. The

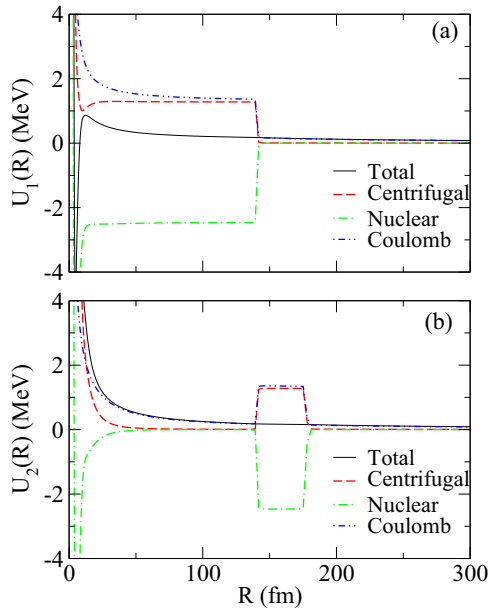

FIG. 3. (Color online) Contributions of the centrifugal potential $\langle\langle\Phi_\nu|\Lambda^2/(2\mu R^2)|\Phi_\nu\rangle\rangle$, the nuclear potentials $\langle\langle\Phi_\nu|\sum_{ij} v_{\alpha\alpha}(r_{ij})|\Phi_\nu\rangle\rangle$, and the Coulomb potentials $\langle\langle\Phi_\nu|\sum_{ij} v_C(r_{ij})|\Phi_\nu\rangle\rangle$ to the two 0^+ lowest potential curves (a) $U_1(R)$ ($\nu = 1$) and (b) $U_2(R)$ ($\nu = 2$), as functions of the hyper-radius R.

radial wave function in the asymptotic region would be obtained analytically as Coulomb functions if the potential curve behaved there as $U_\nu(R) \approx a/R + b/R^2$. If we fit the lowest 0^+ potential curve using this expression at hyper-radii $R \in [400,600]$ fm, we obtain $a = 23.3$ MeV fm and $b = 265$ MeV fm^2. At hyper-radii $R \in [800,1000]$ fm, we obtain $a = 23.1$ MeV fm and $b = 367$ MeV fm^2. This implies that the coefficients a and b are hardly constant even in the asymptotic region, as already noticed by Macek [37]. With short-range interaction, the potentials behave as $U_\nu(R) \sim 1/R^3$ at large distances [38]. The problem is stronger with the Coulomb interaction where couplings appear. In this way, we confirm that the above expression does not hold for three-body systems with both short-range and Coulomb interactions and the hyper-radial wave function cannot be a linear combination of the Coulomb functions in the asymptotic region.

C. ^{12}C spectrum

The bound-state and resonance energies $E(J^\pi_n)$ are obtained by solving the coupled-channel hyper-radial equations in Eq. (9) with the sum over ν truncated at $\nu_{\max}$. In the case of the lowest bound state ($n = 1$) in each symmetry, the upper and lower limits of the energy level can be estimated by the adiabatic and Born-Oppenheimer (BO) solutions, respectively [39,40]. The adiabatic solution corresponds to solving Eq. (9) with only one channel ν, neglecting all coupling elements between different channels, that is, $\mathcal{O}_{\nu l,\nu' l'} = 0$ for $\nu \neq \nu'$. The lowest $\nu = 1$ energy level obtained from Eq. (9) neglecting all coupling elements between different channels gives a variational upper limit to the lowest state energy. One can also solve Eq. (9) by further setting $\mathcal{O}_{\nu l,\nu l'} = 1$, which is equivalent to solving a one-dimensional Schrödinger equation with potential $U_\nu(R)$. This corresponds to the Born-Oppenheimer solution. The lowest resulting energy for $\nu = 1$ gives a rigorous lower limit to the lowest state energy. Finally, solving Eq. (9) with the sum truncated at $\nu, \nu' = \nu_{\max}$ gives variational approximations to the exact energies. These energies will thus converge to the exact energies from above in the limit $\nu_{\max} \to \infty$. Table I summarizes these different levels of approximation to the bound-state and resonance energies of the three-α system in the $J^\pi = 0^+$ and 2^+ symmetries. The lowest state ($n = 1$) in both symmetries is found to converge rapidly with respect to $\nu_{\max}$ and be accurate to more than seven significant digits with $\nu_{\max} \geqslant 20$. In contrast, convergence is a little slower for the $J^\pi_n = 0^+_2$ state, and its resonance position and width are shown to be accurate respectively to 5 and 2 significant digits with $\nu_{\max} \geqslant 20$.

TABLE I. Bound-state and resonance energies $E(J^\pi_n)$ in MeV for the three-α system at various levels of approximation.

J^π_n	0^+_1	0^+_2	2^+_1
BO	-9.414838	$0.2547141 - i1.28 \times 10^{-8}$	-3.045527
Adiabatic	-9.200581	$0.4863017 - i2.15 \times 10^{-5}$	-2.470521
$\nu_{\max} = 5$	-9.300869	$0.3672566 - i4.90 \times 10^{-6}$	-2.837064
10	-9.300921	$0.3669086 - i4.73 \times 10^{-6}$	-2.839370
15	-9.300922	$0.3668920 - i4.70 \times 10^{-6}$	-2.839438
20	-9.300922	$0.3668886 - i4.69 \times 10^{-6}$	-2.839452
25	-9.300922	$0.3668877 - i4.68 \times 10^{-6}$	-2.839452

In the calculations shown in Table I, the hyper-radial FEM-DVR basis functions have been constructed by decomposing the hyper-radial range $0.01 \leqslant R \leqslant 200$ fm into 30 intervals ($N = 31$) and further subdividing each interval with 10-point Gauss-Lobatto quadrature ($\mathcal{M} = 10$). The convergence with respect to the FEM-DVR basis will be checked below by extending the hyper-radial range up to $R = 300$ fm with 6 additional intervals (N then equals 37) or using a larger Gauss-Lobatto quadrature with $\mathcal{M} = 15$. In addition, convergence must also be tested with respect to the minimum scattering energy $E_{\min}$ in the TF-CAP in Eq. (12), although we have used only $E_{\min} = 0.05$ MeV in the calculations shown in Table I. We have therefore focused on the $J^\pi_n = 0^+_2$ state and calculated its resonance position and width for different FEM-DVR bases and different scattering energies, with the fixed number of potential curves $\nu_{\max} = 25$. The results of these convergence tests are shown in Table II. Here, we can see that the 0^+_2 resonance position and width are converged at least to 6 and 2 significant digits, respectively. In conclusion, we have obtained two states with $E(0^+_1) = -9.300922$ MeV, $E(0^+_2) = 0.36689 - i4.7 \times 10^{-6}$ MeV for $J^\pi = 0^+$, and one state with $E(2^+_1) = -2.839452$ MeV for $J^\pi = 2^+$. The 0^+_1 energy is lower than the experimental value of -7.46 MeV [41], whereas the 2^+_1 energy is close to the experimental value of -3.02 MeV. The 0^+_2 Hoyle resonance parameters $E^r(0^+_2) = 0.36689$ MeV and $\Gamma(0^+_2) = 9.4$ eV can be compared with the experimental values, $E^r_{\exp}(0^+_2) = 0.38$ MeV and $\Gamma_{\exp}(0^+_2) = 8.5 \pm 1.0$ eV [41]. We can see that our resonance width agrees with the

TABLE II. Resonance energies $E(0_2^+)$ calculated with different values of the CAP scattering energy $E_{\min}$ and different FEM-DVR bases. $R_{\max}$ is the border of the hyper-radial FEM-DVR grid, and $\mathcal{M}$ is the order of the Gauss-Lobatto quadrature.

$E_{\min}$ (MeV)	$R_{\max}$ (fm)	$\mathcal{M}$	$E(0_2^+)$ (MeV)
0.02	200	10	$0.3668877 - i4.69 \times 10^{-6}$
	300	10	$0.3668877 - i4.69 \times 10^{-6}$
0.05	200	10	$0.3668877 - i4.68 \times 10^{-6}$
		15	$0.3668877 - i4.69 \times 10^{-6}$
	300	10	$0.3668877 - i4.69 \times 10^{-6}$
		15	$0.3668877 - i4.69 \times 10^{-6}$
0.08	200	10	$0.3668878 - i4.69 \times 10^{-6}$
	300	10	$0.3668878 - i4.69 \times 10^{-6}$

experimental one within the experimental uncertainty. This indicates that the width of the Hoyle state is not very sensitive to the short-range α-α potential, as we use an l-independent Ali-Bodmer potential, fitted to the $l = 0$ phase shifts.

D. Discussion of the wave functions

The hyper-radial wave functions at FEM-DVR points can be easily calculated from the coefficient $c_{l\nu}$ in Eq. (7) via $F_\nu(r_l) = \omega_l^{-1/2} c_{l\nu}$. The hyper-radial wave functions associated with the bound and resonance states are shown in Figs. 4(a)–4(c). Figure 4(a) shows the squared first hyper-radial component $|F_1(R)|^2$ for the $J_n^\pi = 0_1^+$ state, while the other components $|F_\nu(R)|^2$ ($\nu = 2,3,\dots$) are too small to be shown here. Figure 4(b) shows the first and second hyper-radial components $|F_\nu(R)|^2$ ($\nu = 1,2$) for the $J_n^\pi = 0_2^+$ state, and the other components are negligibly small. In the same way, the hyper-radial components are shown for $J_n^\pi = 2_1^+$ in Fig. 4(c). For each of the bound and resonance states, the first component $F_1(R)$ clearly dominates over the other ν components $F_\nu(R)$ ($\nu = 2,3,\dots$). The peak position of those dominant components suggests the overall spatial size of the bound and resonance states. Using these hyper-radial wave functions, we can also calculate the root-mean-square (rms) radius of the three-α system, $\sqrt{\langle R^2\rangle}/3^{3/4}$. The averaged squared hyper-radius can be obtained from

$$\langle R^2\rangle = \int dR \int d\Omega \psi^*(R,\Omega) R^2 \psi(R,\Omega) \approx \sum_l \sum_\nu |c_{l\nu}|^2 r_l^2. \tag{17}$$

We obtain $\sqrt{\langle R^2\rangle}/3^{3/4} = 1.78, 3.61$, and 1.91 fm for $J_n^\pi = 0_1^+$, 0_2^+, and 2_1^+ states, respectively. With use of the rms radius of α particle, 1.42 fm, these values indicate the rms radii of the respective states of ^{12}C as 2.28, 3.88, and 2.38 fm.

To obtain more information on the geometric structure of the three-α system, we need to analyze the total wave function $\psi(R,\Omega) \equiv \psi(R,\theta,\varphi,\alpha,\beta,\gamma)$, which is a six-dimensional wave function. Although it is not trivial to deal with a six-dimensional wave function, we can reduce its dimensionality by defining the "three-dimensional (3D) probability density function" as

$$\mathcal{D}(R,\theta,\varphi) = \sin 2\theta \int_0^{2\pi} d\alpha \int_0^{\pi} \sin\beta d\beta \times \int_0^{2\pi} d\gamma |\psi(R,\theta,\varphi,\alpha,\beta,\gamma)|^2, \tag{18}$$

which we can express at hyper-radial FEM-DVR points $R = r_l$ as

$$\mathcal{D}(r_l,\theta,\varphi) = \omega_l^{-1} \sin 2\theta \times \sum_\nu \sum_{\nu'} \sum_K c_{l\nu}^* c_{l\nu'} \phi_{K\nu}^*(r_l;\theta,\varphi) \phi_{K\nu'}(r_l;\theta,\varphi). \tag{19}$$

We introduce the "two-dimensional (2D) probability density functions" by integrating $\mathcal{D}(R,\theta,\varphi)$ over one of the R,θ, and φ coordinates. For example, the 2D probability density function in $\theta\varphi$ space is obtained by integrating over R, i.e.,

$$D(\theta,\varphi) = \int_0^\infty dR \mathcal{D}(R,\theta,\varphi) \approx \sum_l \mathcal{D}(r_l,\theta,\varphi)\omega_l. \tag{20}$$

Contour plots of the 2D probability density functions for $J_n^\pi = 0_1^+$ and 0_2^+ states of the three-α system are presented in Figs. 5(a) and 5(b). The 0_1^+ state is found to maximize around $(R,\theta,\varphi) \approx (3.5\text{fm}, 0.12\pi, 0)$, but spreads widely in the φ direction. In terms of the interparticle distances in Eq. (6), this maximum position corresponds to $(r_{12},r_{23},r_{31}) \approx (2.4,2.4,3.1)$ fm, for which the three-particle system displays an isosceles triangle. The 0_2^+ state also extends widely in the φ direction, but displays two peak positions at $(R,\theta,\varphi) \approx (3\,\text{fm}, 0.12\pi, 0)$ and $(6.5\,\text{fm}, 0.2\pi, 0)$,

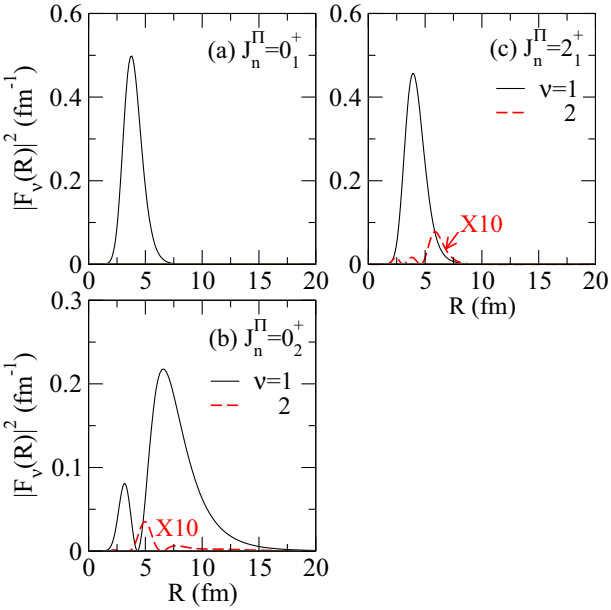

FIG. 4. (Color online) The squared hyper-radial wave functions $|F_\nu(R)|^2$ for the bound and resonance states of the three-α system. (a) $J_n^\pi = 0_1^+$ state: the first $\nu = 1$ hyperradial component in the expansion in Eq. (7) is shown; (b) $J_n^\pi = 0_2^+$ state: the first $\nu = 1$ and second $\nu = 2$ hyper-radial components in the expansion in Eq. (7) are shown respectively as solid and dashed lines; and (c) the same as for panel (b) but for $J_n^\pi = 2_1^+$ state. The $\nu = 2$ components drawn here are magnified 10 times.

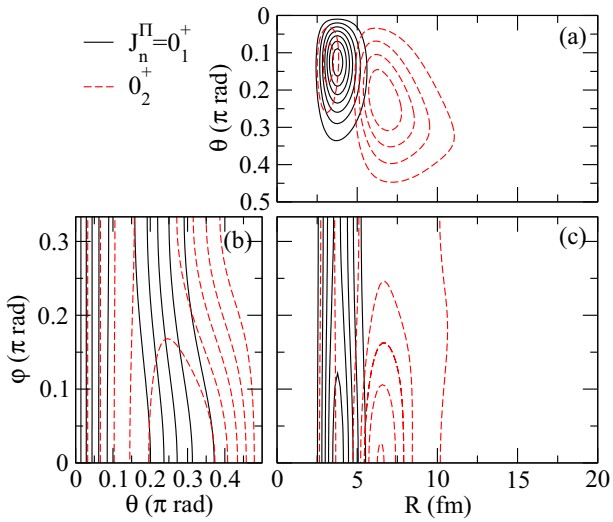

FIG. 5. (Color online) Contour plots of the 2D probability density functions for the $J_n^\pi = 0_1^+$ and 0_2^+ states of the three-α system (a) in $R\theta$ space, (b) in $\theta\varphi$ space, and (c) in $R\varphi$ space. The 0_1^+ state is indicated by solid lines and the 0_2^+ state by dashed lines.

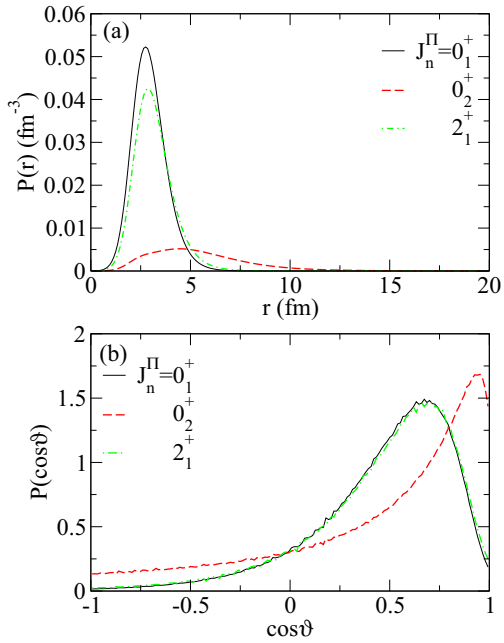

FIG. 6. (Color online) (a) Pair distribution $P(r)$ and (b) angle cosine distribution $P(\cos\vartheta)$ for the $J_n^\pi = 0_1^+$, 0_2^+, and 2_1^+ states.

which correspond respectively to $(r_{12},r_{23},r_{31}) \approx (2.1,2.1,2.7)$ fm and (4.2,4.2,6.2) fm. The peak at smaller R appears to be a consequence of the orthogonality to the 0_1^+ state. The 2_1^+ state can also be analyzed in a similar way. It has the intrinsic structure similar to that of the 0_1^+ state.

These two-dimensional (2D) contour plots do not allow for the direct identification of geometrical configurations. The three-dimensional (3D) probability density functions can be nevertheless be converted easily into one-dimensional (1D) pair and angle distributions. These distribution functions are shown for the $J_n^\pi = 0_1^+$, 0_2^+, and 2_1^+ states in Fig. 6. The pair distribution functions are shown in Fig. 6(a). We calculate r_{12}, r_{23}, and r_{31} as defined in Eq. (6) for each R, θ, and φ and sort the interparticle distances into $P(r)$, which we normalize as $\int_0^\infty P(r)r^2dr = 1$. In Fig. 6(b), we show angle cosine distribution functions $P(\cos\vartheta)$ where ϑ is the bond angle, $\cos\vartheta_{ijk} = (r_{ij}^2 + r_{jk}^2 - r_{ki}^2)/(2r_{ij}r_{jk})$. For each R, θ, and φ, there are three bond angles. We normalize the cosine distribution functions $P(\cos\vartheta)$ as $\int_{-1}^1 P(\cos\vartheta)d(\cos\vartheta) = 1$. The pair distribution functions for the 0_1^+ state is strongly peaked around 2.8 fm. The 2_1^+ state is shown to be peaked almost at the same distance as the 0_1^+ state. In contrast the pair distribution of the 0_2^+ state is much extended, as was pointed out in the literature [42–45]. The pair distribution functions for the 0^+ state obtained in a microscopic three-α cluster model [44] show structure similar to that in Fig. 6(a). By comparing these distribution functions, it is clear that the structure of the 0_2^+ state is quite different from the other two. The angle cosine distribution functions for both the 0_1^+ and 2_1^+ states show broad peaks around $\cos\vartheta \approx 0.67$, or $\vartheta \approx 0.27\pi$. This suggests a scalene triangle that fluctuates around the equilibrium structure, but can be found very often in much distorted shapes. The cosine distribution of the 0_2^+ state is much different from the other two and extends all the way from -1 to $+1$, with a maximum close to, but not exactly, $+1$. Since a cosine of $+1$ corresponds to an angle of zero, this suggests that nearly linear configurations are important. Note that one or two of the three bond angles are zero for a perfect linear configuration. This angle distribution function for the 0_2^+ state shows a very similar nature to the ground state of the atomic ^{4}He trimer in Ref. [46], often characterized as a very weakly bound state.

IV. SUMMARY

In this work, we have developed a method for calculating the bound and continuum energy spectrum of three particles interacting through the Coulomb potential. The method has been applied to calculate the energy spectrum of ^{12}C in a 3α-particle model, focusing on accurate calculation of the Hoyle resonance width of the extremely narrow near-threshold $J_n^\pi = 0_2^+$ state. A combination of the slow variable discretization approach with a complex absorbing potential has allowed us to accurately describe the continuum states of three charged particles and to calculate the resonance width, converging to at least two significant digits, indicating that the near-threshold continuum spectrum is correctly described. This work can be considered as a first step towards accurate description of the famous low-energy triple-α reaction, which is of key importance for stellar nucleosynthesis as a unique possibility for helium burning that allows further synthesis of heavier elements. We are currently working for calculating the triple-α reaction rate.

ACKNOWLEDGMENTS

The work of Y.S. is supported in part by JSPS KAKENHI Grant No. 24540261. He thanks C. H. Greene and D. Blume for several inspiring discussions made during the INIT_14_1 Program "Universality in Few-Body Systems: Theoretical

Challenges and New Directions" (March 10–May 16 2014, University of Washington). H.S. thanks Dr. Emiko Hiyama for her encouragement during this work.

APPENDIX A: SOLUTION OF THE ADIABATIC EQUATION

In order to solve the adiabatic equation (8), we expand the channel functions on Wigner D functions [47]

$$\Phi_\nu^{JM\pi}(R;\Omega) = \sum_K \phi_{K\nu}(R;\theta,\varphi) D^J_{KM}(\alpha,\beta,\gamma). \quad \text{(A1)}$$

The quantum number K denotes the projection of $\vec{J}$ on the body-fixed z axis and takes the values $J, J-2, \ldots, -(J-2), -J$ for the "parity-favored" case, $\pi = (-1)^J$, and $J-1, J-3, \ldots, -(J-3), -(J-1)$ for the "parity-unfavored" case, $\pi = (-1)^{J+1}$, since K should be even for even parity and odd for odd parity [15]. The resulting complex coupled equations in θ and φ are solved by expanding $\phi_{K\nu}(R;\theta,\varphi)$ onto a direct product of fifth-order ($k = 5$) basis splines [48]. We generate basis splines for θ from N_θ mesh points and for φ from N_φ mesh points. Convergence of the adiabatic potential curves with respect to the basis splines can be checked by computing them for different numbers of grid points N_θ and N_φ. For small hyper-radii R, a uniform mesh can be employed; for large R, the mesh may be designed so that it becomes dense around the two-body coalescence points around $(\theta,\varphi) \approx (\pi/2,\pi/3)$, $(\pi/2,\pi)$, and $(\pi/2,5\pi/3)$, where the potential energy surface $V(R,\theta,\varphi)$ changes significantly, as is explained in Sec. III A. All matrix elements are calculated by integrating numerically with shifted and scaled Gauss-Legendre quadratures.

The identical particle symmetry was built into the adiabatic equation (8) via the boundary conditions in φ. For details, see Ref. [47]. In particular, the channel functions must be invariant under the permutation operations $P_{12}P_{31}$ ($\varphi \to \varphi + 2\pi/3$, $\gamma \to \gamma + \pi$) and P_{23} ($\varphi \to 2\pi/3 - \varphi$, $\beta \to \pi - \beta$, $\gamma \to 2\pi - \gamma$). This leads to

$$\Phi_\nu(R;\theta,\varphi,\alpha,\beta,\gamma) = \Phi_\nu(R;\theta,\varphi + 2\pi/3,\alpha,\beta,\gamma + \pi) \quad \text{(A2)}$$

$$= \Phi_\nu(R;\theta,2\pi/3 - \varphi,\alpha,\pi - \beta,2\pi - \gamma). \quad \text{(A3)}$$

These constraints result in boundary conditions at $\varphi = 0$ of

$$(-1)^{J+K}\phi_{-K\nu}(R;\theta,0) = \phi_{K\nu}(R;\theta,0), \quad \text{(A4)}$$

$$(-1)^{J+K+1}\left.\frac{\partial\phi_{-K\nu}}{\partial\varphi}\right|_{\varphi=0} = \left.\frac{\partial\phi_{K\nu}}{\partial\varphi}\right|_{\varphi=0}, \quad \text{(A5)}$$

and those at $\varphi = \pi/3$ of

$$(-1)^{J}\phi_{-K\nu}(R;\theta,\pi/3) = \phi_{K\nu}(R;\theta,\pi/3), \quad \text{(A6)}$$

$$(-1)^{J+1}\left.\frac{\partial\phi_{-K\nu}}{\partial\varphi}\right|_{\varphi=\pi/3} = \left.\frac{\partial\phi_{K\nu}}{\partial\varphi}\right|_{\varphi=\pi/3}, \quad \text{(A7)}$$

and we only need to consider the range $\varphi \in [0,\pi/3]$ (including thus only one two-body coalescence point).

APPENDIX B: TEST CALCULATION OF ^{8}Be(0^+) RESONANCE PARAMETERS

As we mention in the text, the S-wave ^{8}Be resonance for the simple α-α potential ($v_{\alpha\alpha} + v_C$) is described accurately with the help of the TF-CAP. In this appendix we illustrate how the ^{8}Be(0^+) resonance parameters (E_R and Γ) depend on $E_{\min}$ and $R_{\max}$ of the TF-CAP, as well as on the basis dimension N. For this purpose we use here well-known basis functions, the Legendre polynomials, and we expand the S-wave α-α relative motion function as

$$u(r) = \sum_{\ell=0}^{N-1} c_\ell f_\ell(x) \quad \text{(B1)}$$

with

$$f_\ell(x) = \sqrt{\frac{2}{R_{\max}}}[P_\ell(x) + a_\ell^+ P_N(x) + a_\ell^- P_{N+1}(x)]. \quad \text{(B2)}$$

Here $x = 2r/R_{\max} - 1$ and the last two terms of $f_\ell(x)$ are added so as to satisfy the boundary condition, $u(0) = u(R_{\max}) = 0$, which leads to $a_\ell^\pm = -\frac{1}{2}[1 \pm (-1)^{N-\ell}]$. The converged values obtained with large fifth-order basis splines (see text) are $E_R = 88.84$ keV and $\Gamma = 5.66$ eV.

The overlap and kinetic energy matrix elements with the basis (B2) are evaluated analytically. The potential energy matrix element is obtained with a Gauss-Legendre quadrature. We use the potentials (14) and (15) for the α-α interaction, and introduce the CAP (12) with different values for $E_{\min}$ and $R_{\max}$. Table III lists the resonance parameters obtained

TABLE III. Resonance parameters of ^{8}Be (0^+) calculated with Legendre polynomial basis. The exact values are $E_R = 88.84$ keV and $\Gamma = 5.66$ eV.

$E_{\min}$ (MeV)	$R_{\max}$ (fm)	N	E_R (keV)	Γ (eV)
0.15	100	60	88.86	4.75
		80	88.84	4.31
		100	88.84	4.31
0.15	200	80	88.89	8.21
		100	88.84	8.21
		150	88.84	8.20
0.10	200	80	88.88	8.12
		100	88.84	8.08
		150	88.84	8.06
0.05	200	80	88.88	5.24
		100	88.84	5.21
		150	88.84	5.20
0.05	300	100	88.88	5.99
		150	88.84	5.90
		200	88.84	5.90
0.02	200	80	88.88	5.53
		100	88.84	5.50
		150	88.84	5.49
0.02	300	100	88.88	5.78
		150	88.84	5.68
		200	88.84	5.68

for different choices of the CAP parameters. In all cases the resonance energy is found to be stable at least for four digits if N is taken sufficiently large. However, the width depends on a choice of the TF-CAP parameters, which is mainly due to the extremely small ratio of Γ/E_R. Further accuracy is needed to obtain a converged width. Two values of $E_{\rm min}$ (0.15 and 0.10 MeV) are chosen as the case where $E_{\rm min}$ is larger than E_R. In this case we do not obtain the correct width. When $E_{\rm min}$ is chosen to be lower than E_R (0.05 and 0.02 MeV), the calculated width becomes close to the accurate value. In order to reproduce the width accurately we see that $R_{\rm max}$ has to be increased with decreasing $E_{\rm min}$. This is because the de Broglie wavelength corresponding to $E_{\rm min} = 0.15, 0.10, 0.05$ and 0.02 MeV increases to 52.6, 64.5, 91.2, and 144.1 fm, respectively. As a reasonable guide, $R_{\rm max}$ has to be chosen at least of the order of two times the de Broglie wavelength.

[1] H.-M. Müller and K. Langanke, Phys. Rev. C **49**, 524 (1994).
[2] H. Oberhummer, H. Krauss, K. Grün, T. Rauscher, H. Abele, P. Mohr, and G. Staudt, Z. Phys. A: Hadrons Nucl. **349**, 241 (1994).
[3] D. V. Fedorov and A. S. Jensen, Phys. Lett. B **389**, 631 (1996).
[4] S. I. Fedotov, O. I. Kartavtsev, V. I. Kochkin, and A. V. Malykh, Phys. Rev. C **70**, 014006 (2004).
[5] R. Álvarez-Rodríguez, E. Garrido, A. S. Jensen, D. V. Fedorov, and H. O. U. Fynbo, Eur. Phys. J. A **31**, 303 (2007).
[6] S. Ishikawa, Phys. Rev. C **87**, 055804 (2013).
[7] N. B. Nguyen, F. M. Nunes, and I. J. Thompson, Phys. Rev. C **87**, 054615 (2013).
[8] P. Pichler, H. Oberhummer, A. Csótó, and S. Moszkowski, Nucl. Phys. A **618**, 55 (1997).
[9] D. V. Fedorov, A. S. Jensen, M. Thøgersen, E. Garrido, and R. de Diego, Few-Body Syst. **45**, 191 (2009).
[10] F. Hoyle, Astrophys. J., Suppl. **1**, 121 (1954).
[11] O. I. Tolstikhin, S. Watanabe, and M. Matsuzawa, J. Phys. B **29**, L389 (1996).
[12] J. Blandon, V. Kokoouline, and F. Masnou-Seeuws, Phys. Rev. A **75**, 042508 (2007).
[13] C. D. Lin, Phys. Rep. **257**, 1 (1995).
[14] B. R. Johnson, J. Chem. Phys. **73**, 5051 (1980).
[15] B. K. Kendrick, R. T. Pack, R. B. Walker, and E. F. Hayes, J. Chem. Phys. **110**, 6673 (1999).
[16] D. E. Manolopoulos, J. Chem. Phys. **117**, 9552 (2002).
[17] T. Gonzalez-Lezana, E. J. Rackham, and D. E. Manolopoulos, J. Chem. Phys. **120**, 2247 (2004).
[18] Y. Ho, Phys. Rep. **99**, 1 (1983).
[19] S. Ali and A. R. Bodmer, Nucl. Phys. **80**, 99 (1966).
[20] H. Suno, J. Chem. Phys. **134**, 064318 (2011).
[21] H. Suno, J. Chem. Phys. **135**, 134312 (2011).
[22] R. C. Whitten and F. T. Smith, J. Math. Phys. **9**, 1103 (1968).
[23] B. Lepetit, Z. Peng, and A. Kuppermann, Chem. Phys. Lett. **166**, 572 (1990).
[24] R. T. Pack, Chem. Phys. Lett. **108**, 333 (1984).
[25] R. T. Pack and G. A. Parker, J. Chem. Phys. **87**, 3888 (1987).
[26] L. M. Delves, Nucl. Phys. **9**, 391 (1958).
[27] L. M. Delves, Nucl. Phys. **20**, 275 (1960).
[28] M. Abramowitz and I. A. Stegun, *Handbook of Mathematical Functions with Formulas, Graphs, and Mathematical Tables* (Dover, New York, 1964).
[29] D. Manolopoulos and R. Wyatt, Chem. Phys. Lett. **152**, 23 (1988).
[30] M. Zhukov, B. Danilin, D. Fedorov, J. Bang, I. Thompson, and J. Vaagen, Phys. Rep. **231**, 151 (1993).
[31] P. Descouvemont, J. Phys. G **37**, 064010 (2010).
[32] A. Vibok and G. G. Balint-Kurti, J. Phys. Chem. **96**, 8712 (1992).
[33] U. V. Riss and H.-D. Meyer, J. Phys. B **26**, 4503 (1993).
[34] J. G. Muga, J. P. Palao, B. Navarro, and I. L. Egusquiza, Phys. Rep. **395**, 357 (2004).
[35] T. P. Grozdanov and R. McCarroll, J. Chem. Phys. **126**, 034310 (2007).
[36] D. Tilley, J. Kelley, J. Godwin, D. Millener, J. Purcell, C. Sheu, and H. Weller, Nucl. Phys. A **745**, 155 (2004).
[37] J. Macek, J. Phys. B **1**, 831 (1968).
[38] I. J. Thompson, B. V. Danilin, V. D. Efros, J. S. Vaagen, J. M. Bang, and M. V. Zhukov, Phys. Rev. C **61**, 024318 (2000).
[39] A. F. Starace and G. L. Webster, Phys. Rev. A **19**, 1629 (1979).
[40] H. T. Coelho and J. E. Hornos, Phys. Rev. A **43**, 6379 (1991).
[41] F. Ajzenberg-Selove, Nucl. Phys. A **506**, 1 (1990).
[42] M. Kamimura, Nucl. Phys. A **351**, 456 (1981).
[43] Y. Funaki, A. Tohsaki, H. Horiuchi, P. Schuck, and G. Röpke, Phys. Rev. C **67**, 051306(R) (2003).
[44] H. Matsumura and Y. Suzuki, Nucl. Phys. A **739**, 238 (2004).
[45] M. Chernykh, H. Feldmeier, T. Neff, P. von Neumann-Cosel, and A. Richter, Phys. Rev. Lett. **98**, 032501 (2007).
[46] D. Bressanini and G. Morosi, J. Phys. Chem. A **115**, 10880 (2011).
[47] H. Suno, B. D. Esry, C. H. Greene, and J. P. Burke, Phys. Rev. A **65**, 042725 (2002).
[48] C. de Boor, *A Practical Guide to Splines* (Springer, New York, 1978).